Exploring spatiotemporal dynamics in light-dosimetry

S L Hartmeyer[1*], F R Rudawski[2], M Knoop[2] and M Andersen[1]

[1] Laboratory of Integrated Performance in Design (LIPID), School of Architecture, Civil and Environmental Engineering (ENAC), École polytechnique fédérale de Lausanne (EPFL), Lausanne, Switzerland

[2] Chair of Lighting Technology, Institute of Energy and Automation Technology, Technische Universität Berlin, Berlin, Germany

* Corresponding author steffen.hartmeyer@epfl.ch

Abstract. Light-dosimetry aims to measure personal light exposure in real-life settings, allowing to investigate the role of light in visual, physiological, and behavioural processes. One aspect not yet considered in light-dosimetry is the spatial distribution of light in the field of view. Therefore, we developed and tested a novel measurement setup for spatially resolved light-dosimetry. The setup consisted of an industry-standard wide-angle video-radiometer (LMK) worn at the chest and two novel sensor prototypes: a miniature video-radiometer (alphaOmega-meter) and a spectrally resolved dosimeter (Spectrace), both worn at the chest and forehead. The LMK recorded melanopic radiance images at a sampling frequency of 0.5 Hz, achieved with a custom developed algorithm. The alphaOmega-meter recorded α-opic radiance images at 0.1 Hz and Spectrace recorded 14-channel spectral irradiance at 0.03 Hz. A series of test measurements were then conducted in various urban environments, to assess the potential of the measurement setup. Suitable evaluation methods for spatially resolved light-dosimetry data are presented, which may offer novel insights into the effects of light on visual and non-visual responses by enabling a closer approximation of retinal illumination compared to the spatially integrated measurements that are commonly used. Together, this study demonstrates the feasibility of incorporating spatial characteristics in light-dosimetry.

1. Introduction

Light enables visual perception of the world and plays a fundamental role in regulating physiological and behavioural functions, thereby influencing general health and wellbeing. The daily patterns of light we are exposed to are highly complex signals varying over time in intensity, spectral composition, and spatial distribution due to varying lighting conditions and our behaviour and interaction with our environment. Consequently, it is important to measure light exposure in a personalised fashion, also known as light-dosimetry. Light-dosimetry is typically performed with wearable sensors measuring spatially integrated measures such as spectral irradiance or, more commonly, illuminance. The data may then be used to characterize light exposure profiles, validate lighting interventions, or investigate functional relationships between light and physiological or behavioural responses in real-life settings.

Especially the study of such functional relationships has received more attention recently, since light affects several neurophysiological functions such as circadian entrainment, sleep-wake regulation,

melatonin production, and alertness [1]. Previous research has shown that these "non-visual" responses are modulated by spectral and temporal characteristics of light exposure [2]. In addition, findings from experiments illuminating different retinal regions (i.e., nasal vs. temporal, superior vs. inferior) suggests that the spatial distribution of light in the visual field modulates non-visual responses. [3–7].

Based on these modulating effects, it was recently recommended to report the spatial distribution of lighting conditions in experimental studies on non-visual effects of light [8]. These recommendations, however, are not directly applicable to field studies involving light-dosimetry. In general, studies in the field differ substantially from laboratory studies, as the experimental procedures and settings are less controlled: subjects are measured in real-life environments, usually over prolonged periods (e.g., several days), in which they may encounter diverse lighting conditions with frequent changes of the visual scene due to movement and changes in viewing direction. Moreover, the availability of wearable sensors for measuring the spatial distribution of light is currently limited, especially for α-opic quantities relevant for research on the non-visual effects of light [9].

Given these challenges, it is not clear to what extent and under what circumstances, spatially resolved measurements can be relevant for light-dosimetry, especially in the context of research on the non-visual effects of light [10][11]. To start addressing this issue, we developed a light-dosimetry setup enabling measurement of the spatial light distributions encountered by a person in real-life settings. We then performed a series of test measurements to explore the potential of the setup to measure the spatiotemporal dynamics of personal light exposure in different urban environments. Based on the test measurements, we present methods for the processing and analysis of spatially resolved light-dosimetry data considering different possible research objectives.

2. Materials and method

2.1. Objectives

Conceptually, the setup described here was developed with the aim to measure spatially resolved personal light exposure data for research in the context of the non-visual effects of light, therefore, melanopic and α-opic quantities were recorded. Furthermore, the setup was configured to be able to compare measurements at the forehead and the chest (also discussed in [10]).

2.2. Measures and setup

The novel measurement setup developed for this study consisted of several sensors controlled by a laptop computer and powered by a portable battery stored in a backpack (Figure 1a). With this setup, two types of measures were recorded: (1) *spatially resolved* and (2) *spatially integrated* measures (Table 1). The setup was configured to measure at the forehead and at the chest. In the following, the specific data collection procedures for each measure are explained in more detail. The scripts with the implementation of the described procedures are openly available on doi.org/10.5281/zenodo.7852031.

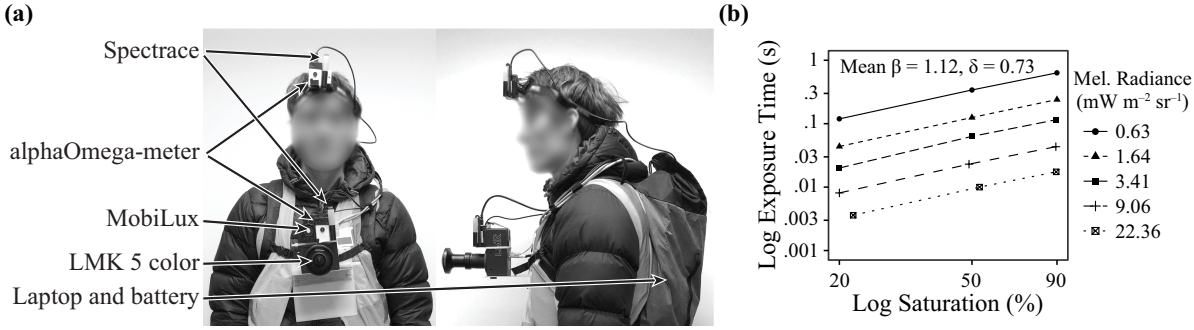

Figure 1. (a) Overview of the measurement setup; **(b)** log-log linear relationship between saturation and exposure time for images with the LMK camera at different melanopic radiance levels from which the coefficients for the exposure time adjustment algorithm were derived: mean slope β and mean difference δ between exposure times for 20% and 90% saturation.

Table 1. Characteristics of the measurement setup.

Sensor	Position	Measure	Sampling frequency	Field of view	Image resolution	Dynamic range
LMK camera	Chest	Melanopic radiance distribution[1]	0.5Hz	180°	243×203 px	1:1100
alphaOmega-meter	Chest, Forehead	Estimated α-opic radiance distribution[1]	0.1Hz	120°×100°	160×120 px	1:10000
Spectrace	Chest, Forehead	Spectral irradiance[2]	0.03Hz	180°	n/a	n/a
MobiLux	Chest	Illuminance[2]	0.5Hz	180°	n/a	n/a

[1] Spatially resolved
[2] Spatially integrated

2.2.1. Spatial melanopic radiance distribution (LMK). The spatial melanopic radiance distribution (or melanopic radiance image) was measured at the chest with a calibrated LMK 5 color (TechnoTeam Bildverarbeitung GmbH, Ilmenau, Germany) video radiometer equipped with a 180° fisheye lens, using its integrated melanopic filter characterised by a peak at 490 nm and 85 nm full width at half maximum.

Images were captured as single exposures with a resolution of 2428×2034 pixels and a dynamic range of 1:1100, with exposure times varying between 0.001–1 s. A neutral density filter with 8.25% transmittance was used to increase exposure time for preventing erroneous measurements due to electric light flicker and to avoid overexposure under bright daylight conditions.

Successive single images were captured with a sampling interval of ~2 s (0.5Hz), depending on the exposure and processing time. Due to the limited dynamic range of single images, a custom algorithm was implemented for dynamically adjusting the exposure time to maintain high image saturation under varying light levels: For each image, the exposure time T was adjusted based on the previous image's saturation S, to reach a target saturation S_{target} of 90%, given the log-log linear relationship with slope β (Figure 1b). If between images a change in ambient illuminance ΔE of more than one log-unit occurred or if the previous image's saturation was lower than 20% or higher than 117% (the maximum saturation threshold), the exposure time was adjusted by δ (i.e., the difference in exposure times for 20% and 90% saturation for a given scene). Ambient illuminance was measured with a MobiLux (Czibula & Grundmann GmbH, Berlin, Germany) illuminance meter. The coefficients β and δ were derived from measurements of image saturation for different exposure times at a range of melanopic radiances (0.6–22.3 W m^{-2} sr^{-1}) given by a tuneable LED light source (Figure 1b). Exposure times were limited to 0.001–1 s, to avoid extreme underexposure for scenes with very bright light sources and overly long exposure for very dark scenes. Mathematically, the algorithm can be defined as in equation (1):

$$\log_{10} T_{new} = \begin{cases} \log_{10}(T) - \delta & \text{if } \log_{10}\Delta E \leq -1 \text{ or } S < 20 \\ \log_{10}(T) + \delta & \text{if } \log_{10}\Delta E \geq 1 \text{ or } S \geq 117 \\ \beta \cdot \log_{10}(S_{target} \cdot T \cdot S^{-1}) & \text{otherwise} \end{cases}, \text{ with } \begin{matrix} T \in [0.001, 1] \\ \beta = 1.12 \\ \delta = 0.73 \\ S_{target} = 90 \end{matrix} \quad (1)$$

To reduce the size of the generated data, captured images were downscaled and stored with a resolution of 243×204 pixels. For later analyses, images were re-scaled to the original resolution. Resizing was performed using the *imresize* function (MATLAB R2021a, MathWorks Inc., Natick, USA) with bilinear interpolation and antialiasing. The mean pixel-to-pixel error after resizing was 2–50%, depending on the image noise; however, the error in total irradiance did not exceed 1%, even for very noisy images. The algorithm was implemented in MATLAB, using the ActiveX interface for controlling the camera software LabSoft (TechnoTeam Bildverarbeitung GmbH, Ilmenau, Germany).

2.2.2. Spatial α-opic radiance distribution (alphaOmega-meter). The spatial α-opic radiance distribution was measured at the chest and forehead with a novel spatially resolved dosimeter prototype,

developed at the TU Berlin. This compact low-budget wearable sensor consists of a wide-angle miniature camera connected to a micro-controller and a SD card for data storage. High-dynamic-range (HDR) images are created on-board from the sensor's raw data by combining the pixels from images with different exposure times, enabling a dynamic range of 1:10000. To reduce memory load and processing time, images were processed and stored with a resolution of 160×120 pixels. The sampling interval was determined by the HDR image creation time, which was ~10 seconds (0.1 Hz).

The recorded HDR images were converted post-hoc to α-opic and photopic radiance images in MATLAB, using linear combinations of the three colour channels. Calibration was performed using a Specbos 1211 (JETI Technische Instrumente GmbH, Jena, Germany) reference spectrometer and a LED OL490 (Gooch & Housego, Ilminster, UK) spectrally tuneable light source. A detailed description of the device and the calibration procedure will be covered in a separate article, currently in preparation.

2.2.3. Spectral irradiance (Spectrace). Spectral irradiance across 14 channels within the visible range was measured at the chest and the forehead with the Spectrace dosimeter prototype developed at EPFL [12]. Measurements were conducted with a sampling interval of 30 s (0.03Hz). The devices were calibrated using a Flame (Ocean Optics Inc., Orlando, FL, USA) reference spectrometer and a Spectra Tune Lab (Ledmotive, Barcelona, Spain) spectrally tuneable light source.

3. Data analysis and test measurements

3.1. Analysis of spatially resolved light-dosimetry data

The data generated with the measurement setup consists of timeseries of spatial radiance distributions and spectral irradiance in different environments. While the spectral irradiance data can be analysed with timeseries analysis methods common in light-dosimetry, as described in a recent comprehensive review [11], the spatial light data first needs to be quantified before timeseries analysis can be applied, as illustrated in Figure 2. The main challenge herein is the selection of an appropriate way to quantify the spatial distribution, which depends on the research focus. For example, for research on visual effects, it might be of interest to quantify the global contrast per image or detect glare sources. Moreover, as the data enables an approximation of the distribution of light on the retina, photoreceptor receptive fields (e.g., of ipRGCs) or entire retinal regions (e.g., nasal, temporal, superior, inferior) can be modelled to examine the effects of spatial distribution on non-visual responses and calculate spatially weighted light exposure. The data can also reveal the arrangement of a person's lighting environment and their interaction with it, for example, the position of light sources in the field of view at the workplace.

3.2. Example of spatially resolved light-dosimetry data

As a proof of concept for the pertinence of the framework depicted in Figure 2, test measurements with the developed setup were conducted across eight continuous periods in December 2021, comprising different environmental settings. Each measurement (i.e., radiance image, Figure 2a) was categorized in terms of setting (e.g., bus, street, office etc.) and time of day (day, night), as shown in Figure 3a.

For research on the non-visual effects of light, it may be of interest to examine the difference in melanopic irradiance across hemifields (i.e., regional irradiance, Figure 2b), approximating the illumination of different retinal regions over time (i.e., timeseries of regional irradiance, Figure 2d), and how these differences vary across study environments. For example, these timeseries of hemifield differences, such as shown in Figure 3b, can indicate the overall spatiotemporal variability, as well as where most of the light in a specific environment originated from; here, from the left during the day and from the right during the night/electric lighting. When aggregating these timeseries (Figure 2e), the mean absolute difference (i.e., ignoring direction of difference) between hemifields can be compared across environments, or the theoretical effect of hemifield differences "cancelling out" over time (i.e., considering direction of difference), as shown in Figure 3c. Here the example data shows how in daytime urban outdoor environments with open view (street open day) absolute differences between left and right hemifields were lower than in indoor and dense urban environments. However, in environments

with variability due to changes in viewing direction or movement, left and right hemifield differences somewhat cancel out when aggregating over time. This may be a consideration for selecting the sensor location, given the higher variability of measurements at the head compared to the chest (Figure 3d).

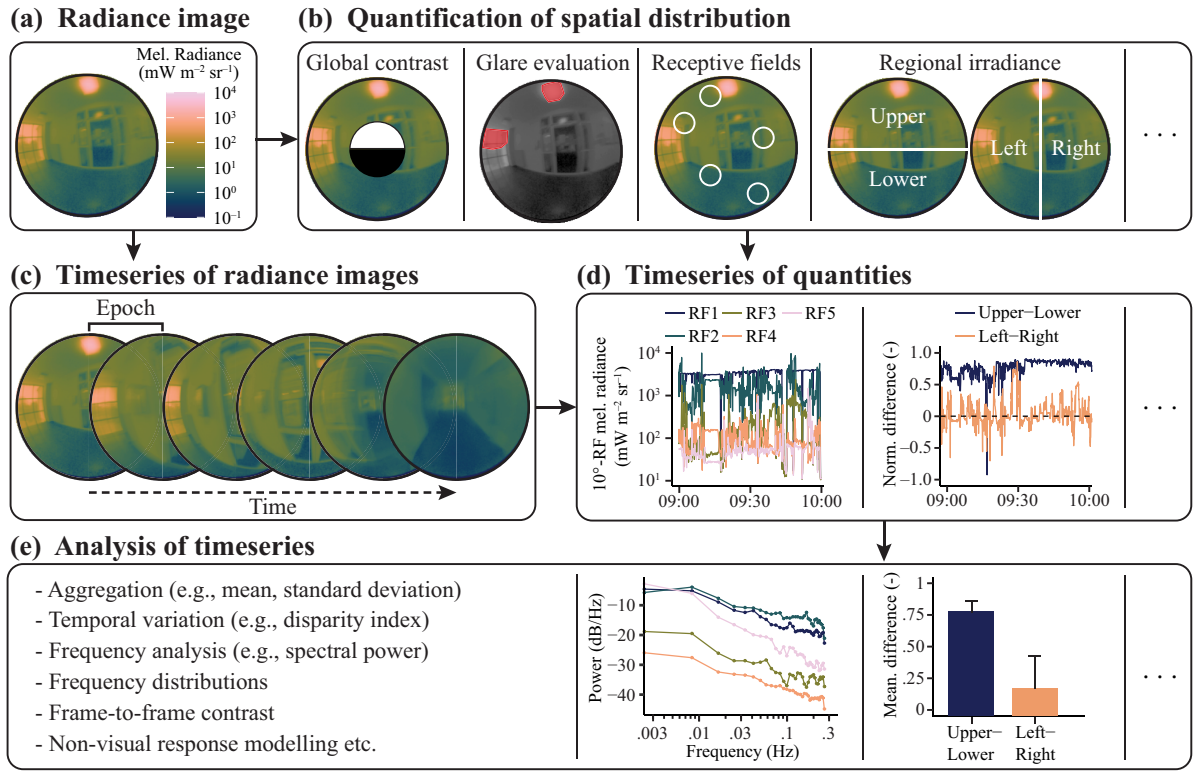

Figure 2. Spatially-resolved light-dosimetry data and potential analysis methods: **(a)** each measurement sample is a radiance image (here melanopic radiance, plotted using the *batlow* perceptually uniform colour scale [13]), **(b)** which can be quantified in different ways; **(c)** as images are sampled over time at a given interval (epoch), **(d)** quantification of each sample results in a timeseries of the chosen quantiy, **(e)** which can then be further aggregated/analysed by various timeseries analysis methods and compared across independent study variables.

4. Discussion and Conclusion

In the present study, a novel measurement setup was developed to collect spatially resolved light-dosimetry data with the aim to assess its potential for future research. We show that the data collected with this setup can provide new insights into personal light exposure patterns. However, given the substantial amount of information this data provides, the main challenge is selecting an appropriate way to quantify the spatial distribution, which strongly depends on the research focus. As described before, spatially resolved light-dosimetry data may be of particular relevance for research on non-visual effects of light. For instance, this data could be recorded alongside physiological or behavioural responses to assess the effects of spatial distribution in real-life settings or may be used to simulate responses once the mechanisms underlying non-visual effects are better understood. Furthermore, the spatially resolved light data allow to better characterise lighting environments and may be used together with spectral measurements to validate lighting designs or assess potential for interventions.

The setup presented here was specifically developed to record melanopic radiance images at a relatively high temporal frequency and configured to compare different measurement positions. While this setup is not suitable for larger scale field-studies due to the total cost of the equipment and the intrusiveness of the setup, it can be easily reconfigured to only use low-cost wearable sensors such as the alphaOmega-meter and Spectrace, which are able to capture α-opic quantities. Note that the

quantities recorded are an important limitation: while several miniature HDR video cameras are available, they often only record luminance images, which is not sufficient for research on non-visual effects of light. As more wearable video-radiometers measuring α-opic quantities at higher temporal resolutions are developed in the future, spatially resolved light-dosimetry may become even more accessible and unveil new insights into the role of light in human health and well-being.

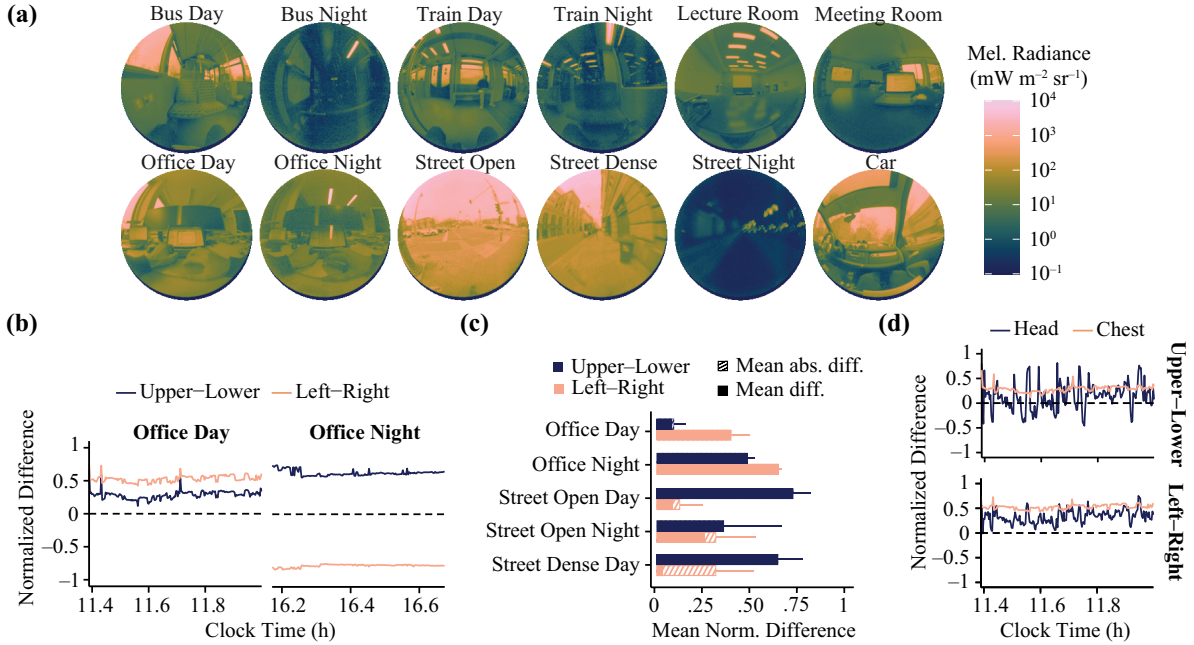

Figure 2. **(a)** Example melanopic radiance images (LMK) for different environments; **(b)** timeseries of normalized differences in melanopic irradiance between hemifields (alphaOmega-meter); **(c)** mean of (absolute) normalized hemifield differences; **(d)** hemifield differences at head and chest.

Funding

This research is part of the LIGHTCAP project, that has received funding from the European Union's Horizon 2020 research and innovation programme under the Marie Sklodowska-Curie Innovative Training Networks (ITN) grant agreement No. 860613.

References

[1] Gooley JJ, Lu J, Chou TC, Scammell TE and Saper CB 2001 *Nat. Neurosci.* **4** 1165

[2] Prayag AS, Münch M, Aeschbach D, Chellappa SL and Gronfier C 2019 *Clocks Sleep* **1** 193–208

[3] Rea MS, Nagare R and Figueiro MG 2021 *Neurobiol. Sleep Circadian Rhythms* **10** 100066

[4] Rüger M, Gordijn MCM, Beersma DGM, de Vries B and Daan S 2005 *J. Biol. Rhythms* **20** 60–70

[5] Visser EK, Beersma DGM, Daan S 1999 *J. Biol. Rhythms* **14** 116–21

[6] Glickman G, Hanifin JP, Rollag MD, Wang J, Cooper H and Brainard GC 2003 *J. Biol. Rhythms* **18** 71–9

[7] Lasko TA, Kripke DF, and Elliot JA 1999 *J. Biol. Rhythms* **14** 122–5

[8] Knoop M, Broszio K, Diakite A, Liedtke C, Niedling M, Rothert I, Rudawski F and Weber N 2019 *LEUKOS* **15** 163–79

[9] CIE 2018 *International Standard CIE S 026/E:2018* (Vienna: CIE)

[10] Hartmeyer SL, Webler FS and Andersen M 2022 *Light. Res. Technol.* **0** 1–23

[11] Hartmeyer SL and Andersen M 2023 *Light. Res. Technol.* **0** 1–29

[12] Webler FS, Chinazzo G and Andersen M 2021 *J. Phys.: Conf Ser.* **2042** 012120

[13] Crameri F, Shephard GE and Heron PJ 2020 *Nat Commun.* **11** 5444